New Journal of Physics
The open-access journal for physics

Coherent collapses of dipolar Bose–Einstein condensates for different trap geometries

J Metz[1], T Lahaye[1], B Fröhlich[1], A Griesmaier[1], T Pfau[1,5], H Saito[2], Y Kawaguchi[3] and M Ueda[3,4]

[1] Physikalisches Institut, Universität Stuttgart, Pfaffenwaldring 57, 70569 Stuttgart, Germany
[2] Department of Applied Physics and Chemistry, The University of Electro-communications, Tokyo 182-8585, Japan
[3] Department of Physics, University of Tokyo, Tokyo 113-033, Japan
[4] ERATO Macroscopic Quantum Project, JST, Tokyo 113-8656, Japan
E-mail: t.pfau@physik.uni-stuttgart.de

New Journal of Physics **11** (2009) 055032 (11pp)
Received 19 December 2008
Published 14 May 2009
Online at http://www.njp.org/
doi:10.1088/1367-2630/11/5/055032

Abstract. We experimentally investigate the collapse dynamics of dipolar Bose–Einstein condensates of chromium atoms in different harmonic trap geometries, from prolate to oblate. The evolutions of the condensates in the unstable regime are compared with three-dimensional simulations of the Gross–Pitaevskii equation including three-body losses. In order to probe the phase coherence of collapsed condensates, we induce the collapse in several condensates simultaneously and let them interfere.

Contents

[5] Author to whom any correspondence should be addressed.

1. Introduction

A collapse is a fast, collective phenomenon consisting of the destruction of a multi-particle system happening abruptly on the timescale that governs the 'usual dynamics'. One example is the collapse of the gravitational core, initiating a supernova. Happening within milliseconds, the duration of the collapse is negligible compared to any of the timescales related to the preceding fusion stages [1].

In contrast to a supernova, where the experimenter is only an observer, Bose–Einstein condensates (BECs) are excellent adjustable systems. Tailoring both the external confining potential and the interaction between the atoms allows us to control the properties of the condensate. It is an ideal system to study not only problems of condensed matter physics [2]–[9] but also the dynamics of a collapse as well.

Collapsing condensates were first observed in ^{7}Li [10] and ^{85}Rb [11]. Both systems are characterized by the contact interaction, which is described by a single parameter, the s-wave scattering length a. From a simple model [12] minimizing the Gross–Pitaevskii energy functional using a Gaussian ansatz for the wave function, one can understand the instability threshold. The energy functional consists of three terms: (i) the kinetic energy, which, in the sub-micro-kelvin range of almost pure condensates, is equal to the quantum pressure (arising from the Heisenberg uncertainty principle in the trap potential), (ii) the harmonic trapping potential and (iii) the interaction energy. For repulsive contact interaction ($a > 0$) a global minimum exists, and the condensate is stable. For small enough attractive interactions ($a < 0$), only a *local* minimum exists at finite size; the condensate is metastable. Finally, for sufficiently attractive interaction the local minimum vanishes. The potential energy of the BEC can be lowered without limit by contraction. Thus, the condensate is unstable.

As the density increases, this model is too simple for describing the physics of the unstable cloud—atom losses due to three-body collisions have to be included. Being negligible at low densities, the three-body collision rate rapidly increases as the cloud shrinks. A three-body collision allows for the production of a dimer, where the third contributing atom is needed to fulfill energy and momentum conservation. The binding energy that is absorbed by the atom and molecule in the form of kinetic energy is sufficient for both to escape from the trap. Hence, instead of reaching a fully contracted 'point-like' state, more and more atoms are lost, so that eventually the quantum pressure dominates over the remaining interaction energy. The dynamics inverts and the atoms accelerate outwards to the *new* equilibrium state. Because the three-body losses have changed the total energy, this new equilibrium state differs from the initial one.

Inducing the collapse in a condensate with non-negligible dipolar interactions changes the dynamics completely. Whereas the contact interaction is short range and spherically symmetric, the dipolar interaction is long range and cylindrically symmetric (partially attractive and partially repulsive). Therefore, dipolar condensates exhibit many novel phenomena even in non-collapsing systems [13]–[25].

The anisotropy of the dipolar interaction can also be used to change the mechanism for the collapse—either driving or stabilizing the collapse: in a cigar-shaped trap with the dipoles oriented along the long axis, the atoms experience predominantly the attractive part of the dipolar mean-field potential [26]. Hence, the collapse is *driven* by the dipolar interaction, whereas the contact interaction stabilizes the condensate. The instability occurs at positive scattering length. This situation is reversed if the dipoles are confined in a pancake-shaped trap. Now their dipolar interaction is essentially repulsive. The dipolar interaction *stabilizes*

the condensate and the condensate is able to withstand negative scattering lengths for which a purely contact interacting BEC would have already become unstable [26]. The instability occurs at negative scattering length. This simple consideration strongly suggests that different trap geometries result in different collapse dynamics.

In this paper, we study the collapse of a chromium condensate under the influence of magnetic dipole interaction [26]–[28]. After describing our experimental procedure for inducing the collapse, we compare the experimental data for different trapping potentials with three-dimensional (3D) simulations of the Gross–Pitaevskii equation (GPE) including three-body losses. We show that this model provides a good description of the experimental data. This is not clear *a priori* as one might expect that the collapse dynamics induces many-body quantum correlations, while the GPE is a mean-field description, not taking correlations into account. Finally, we prove that the collapsed atomic cloud contains a remnant *condensate* by probing its phase coherence. Although simulations for purely contact interacting BECs have shown [29] that the observed bursts and jets of a collapsing condensate should be coherent, this had not been tested experimentally to date.

2. Experimental sequence for producing collapsing dipolar condensates

In order to create a condensate dominated by the dipolar interaction, we exploit the broadest of the observed Feshbach resonances in ^{52}Cr [30]. In the vicinity of this Feshbach resonance, the scattering length varies with the applied magnetic field B as [31]

$$a(B) = a_{\mathrm{bg}}\left(1 - \frac{\Delta B}{B - B_0}\right), \tag{1}$$

where $B_0 \approx 589.1$ G is the position of the Feshbach resonance, $\Delta B = (1.4 \pm 0.1)$ G is its width and $a_{\mathrm{bg}} \approx 100\, a_{\mathrm{Bohr}}$ is the background scattering length with a_{Bohr} being the Bohr radius. The magnetic field is directed along the z-direction and determines the orientation of the dipoles. Using the experimental procedure described in [26], a condensate of approximately 50 000 atoms is formed in a crossed far-detuned optical dipole trap at $a_{\mathrm{evap}} \approx 85 a_{\mathrm{Bohr}}$ above the Feshbach resonance. We then shape the external confining potentials to obtain the desired ratio of the trapping frequencies $\lambda := \omega_z/\omega_y$ by adjusting the power in the crossed dipole trap and superimposing (only for pancake-shaped traps $\lambda > 1$) an additional 1D optical lattice along the z-direction. The superimposed lattice is formed by two far-detuned beams (wavelength $\lambda_{\mathrm{laser}} = 1064$ nm) crossing under a small angle ($\vartheta \approx 8^\circ$), as shown in figure 1. This results in a relatively large spacing of $d_{\mathrm{lat}} = \lambda_{\mathrm{laser}}/[2\sin(\vartheta/2)] = (7.4 \pm 0.2)\ \mu$m between neighboring lattice sites.

We first adiabatically ramp the current in the offset coils linearly in 8 ms to a scattering length a_{i} close to the point where the collapse occurs, and wait for 1 ms for the eddy currents (mainly due to copper gaskets in our experimental chamber) to fade out. Thus, the magnetic field $B(t)$ at the position of the atoms does not follow the ramp instantaneously, but must be calculated according to the equation

$$B(t) = \tilde{B}(t) - \tau_B \dot{B}(t), \tag{2}$$

where $\tilde{B}(t)$ is the magnetic field produced by the offset coils (changed linearly during ramps) and $\tau_B = (0.57 \pm 0.05)$ ms is the $1/e$ lifetime of the eddy currents, measured by Zeeman spectroscopy [32]. After 1 ms of waiting time at a_{i}, we start a second ramp from a_{i} to $a_{\mathrm{f}} < a_{\mathrm{crit}}(\lambda)$, where $a_{\mathrm{crit}}(\lambda)$ is the critical scattering length for the given trapping potential [26],

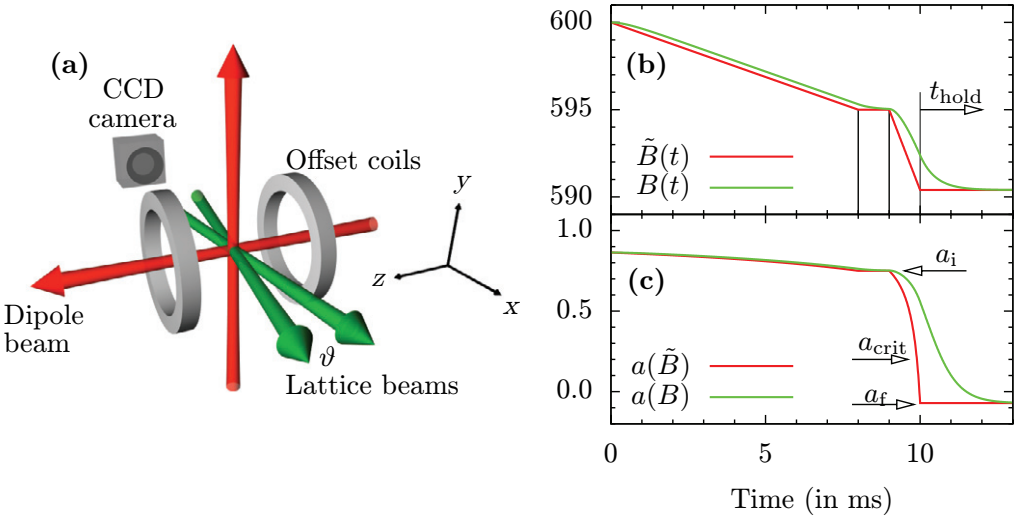

Figure 1. (a) Experimental setup: we realize different confining potentials by superimposing a 1D optical lattice (green) and a crossed dipole trap (red). The offset coils produce the magnetic field for the Feshbach resonance. (b) Eddy currents retard the magnetic field B at the position of the atoms (green) with respect to the ramps of the offset coils (red). The time $t_{\rm hold}$ is defined as the additional holding time of the atoms in the optical trap after finishing the second magnetic field ramp, before the time-of-flight. (c) The corresponding scattering length in units of $a_{\rm bg}$.

so that the collapse occurs. We hold the atoms in the trap for an additional time $t_{\rm hold}$ at $a_{\rm f}$ before releasing them and taking a time-of-flight image. In order to get the maximal absorption cross section, we split the time-of-flight into two parts: a first one, lasting for 4 ms, at the magnetic field corresponding to $a_{\rm f}$ (in order not to disturb the dynamics), and a second part, lasting again for 4 ms, where the large magnetic field along z is replaced by a field of 11 G along the x-direction. We checked that this procedure does not disturb the image.

The observed integrated density distribution is bimodal and consists of a broad isotropic thermal cloud and an anisotropic remnant BEC (see e.g. figure 1(b) of [32]). Because the size of the thermal cloud as well as its atom number does not depend on $t_{\rm hold}$, it is unlikely to contribute to the collapse dynamics. In the following, we have subtracted it from the images to increase the contrast.

3. Collapse dynamics for different trap geometries

The anisotropic character of the dipolar interaction (dipoles that are side-by-side repel each other, whereas dipoles in a head-to-tail configuration attract each other) has a strong effect on the stability of a dipolar condensate: varying the geometry of the confining harmonic trap from prolate to oblate (the symmetry axis being the one along which the dipoles are aligned) stabilizes the condensate, as was demonstrated experimentally in [26]. Our previous experimental study of the collapse dynamics of a dipolar condensate [32] was restricted to an almost spherical trap; in the following, we study the influence of the trap geometry on the collapse dynamics.

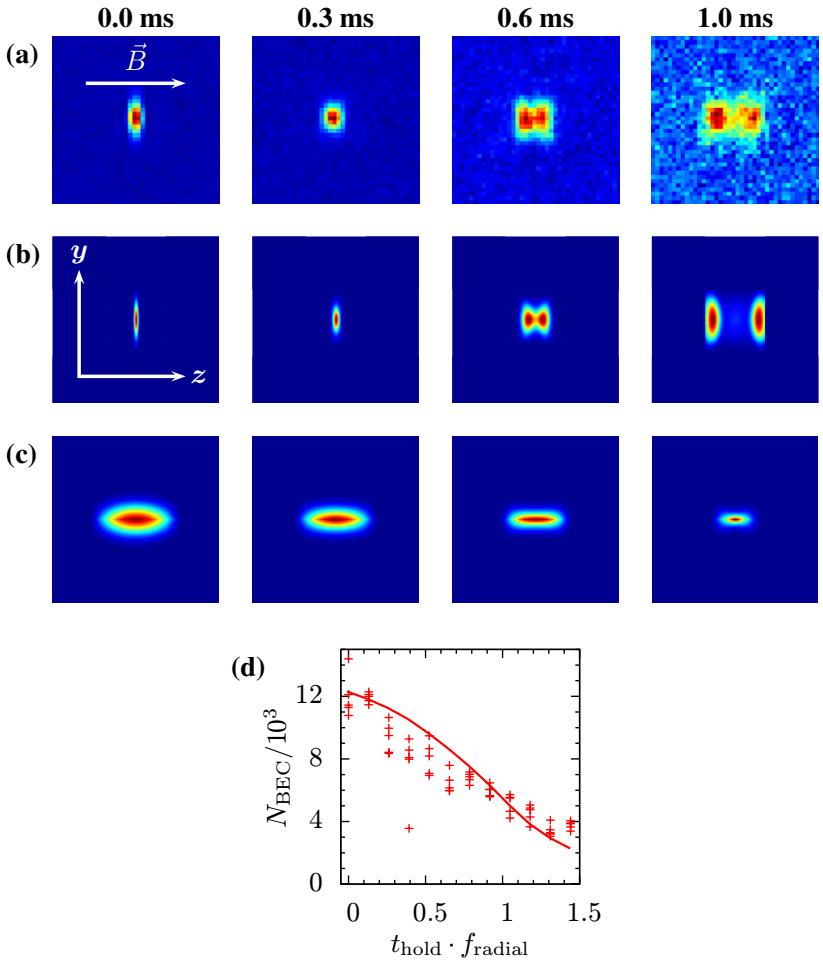

Figure 2. Comparison of the experimental absorption images (a) with the simulations (b) for a cigar-shaped trap with trapping frequencies $(f_x, f_y, f_z) \approx (1312, 1311, 161)$ Hz and trap ratio $\lambda \approx 0.12$. Each image shows the averaged column density of five pictures after 8 ms of time-of-flight. The field of view is $250 \times 250\,\mu\mathrm{m}^2$. The final value of a_{f} was $(8 \pm 3)a_{\mathrm{Bohr}}$ (also in the simulation). (c) Simulated in-trap absorption images. The field of view is $(y, z) = (4.8, 25)\,\mu$m. (d) The remnant condensate atom number N_{BEC} for different holding times t_{hold} in units of the radial trap period $\tau = 1/f_{\mathrm{radial}} \simeq 0.76$ ms. The solid line is the result of the numerical simulation (see text), without any adjustable parameter.

3.1. Prolate traps

For purely contact interacting condensates, the timescale that governs the 'usual dynamics' is set by the largest trap frequency. In contrast, for dipolar condensates this timescale is given by the largest *radial* trap frequency $\tau := 1/f_{\mathrm{radial}}$, because the collapse is induced in this direction [32].

Figure 2 presents the collapse of a dipolar condensate in a highly elongated prolate trap ($\lambda \simeq 0.12$). Here we ramp from an initial scattering length $a_{\mathrm{i}} = (35 \pm 2)a_{\mathrm{Bohr}}$ to $a_{\mathrm{f}} = (8 \pm 3)a_{\mathrm{Bohr}}$, which lies below the critical scattering length $a_{\mathrm{crit}} \approx 12a_{\mathrm{Bohr}}$. On the timescale of

the radial trap period $\tau \approx 0.76\,\mathrm{ms}$, the condensate only starts to split. This is explicitly shown in figure 2(d): the atom number does not drop 'abruptly' to its final value, but instead changes linearly on the timescale τ. Therefore, in the case of figure 2 we observe only a 'moderate' collapse.

Each panel of figures 2(a) and (b) presents the integrated column density $\int \mathrm{d}\,x\,|\psi(\vec{r},t)|^2$ of an absorption image after 8 ms of free expansion. While the upper row shows the experimental data, the lower row is obtained from a numerical simulation of the 3D Gross–Pitaevskii equation

$$\mathrm{i}\hbar\frac{\partial}{\partial t}\psi(\vec{r},t) = \left\{-\frac{\hbar^2}{2m}\nabla^2 + V_{\mathrm{trap}} + \int U(\vec{r}-\vec{r}',t)|\psi(\vec{r}',t)|^2\,\mathrm{d}^3r' - \frac{\mathrm{i}\hbar L_3}{2}|\psi(\vec{r},t)|^4\right\}\psi(\vec{r},t)$$

with the contact and dipolar interactions

$$U(\vec{r},t) = \frac{4\pi\hbar^2 a(t)}{m}\,\delta(\vec{r}) + \frac{\mu_0\mu^2}{4\pi}\,\frac{1-3\cos^2\theta}{|\vec{r}|^3},$$

where m is the atomic mass, μ_0 the magnetic permeability of vacuum, $\mu = 6\mu_{\mathrm{Bohr}}$ the magnetic moment of chromium and θ the angle between $\vec{r}$ and the magnetic field $\vec{B} \parallel \vec{e}_z$. The imaginary term describes the atom losses. The simulations contain *no* free parameter, as the three-body coefficient $L_3 = 2\times10^{-40}\,\mathrm{m^6\,s^{-1}}$ was estimated from measurements. Details of the simulations are given in [32].

Figure 3 shows the collapse in a cigar-shaped trap with trapping frequencies $(f_x, f_y, f_z) \approx (650, 520, 400)$ Hz, corresponding to $\lambda \simeq 0.7$, and radial trapping period $\tau \simeq 1.7$ ms. We start with $N_{\mathrm{BEC}} = 13\,500 \pm 1500$ atoms before ramping the scattering length from $a_{\mathrm{i}} = (35\pm2)a_{\mathrm{Bohr}}$ to $a_{\mathrm{f}} = (8\pm3)a_{\mathrm{Bohr}}$, which lies $4a_{\mathrm{Bohr}}$ below the critical scattering length. The absorption images indicate three different stages: firstly, for $t_{\mathrm{hold}} = 0$ ms, the condensate is strongly elongated along the magnetic field direction, demonstrating strong dipolar interactions [28]. Secondly, we observe a change in ellipticity after $0.4\,\mathrm{ms} \approx 0.3\,\tau$. This is a consequence of the radial implosion and subsequent explosion (a stable, cigar-shaped dipolar condensate does not invert its ellipticity during the free expansion [28]). Thirdly, we observe a splitting of the condensate in the axial direction as in figure 2, but now after $0.8\,\mathrm{ms} \approx 0.5\tau$. For longer holding times the splitting becomes more prominent, but the dynamics is already complete after half a trapping period. This is shown in figure 3(d). The remnant atom number $N_{\mathrm{BEC}}(t)$ drops from 12 000 to 4000 within this timescale. Note that, for this figure (and only this one), the simulation results are in better agreement with the data when performed with $a_{\mathrm{f}} = 2a_{\mathrm{Bohr}}$ (the results shown in figure 3 are for this value of a_{f}). This slight discrepancy is most probably due to a slow drift of the magnetic field that occurred between the data acquisition and the calibration of the scattering length (the calibration procedure, described in detail in [28], requires the accumulation of a large quantity of data).

3.2. Oblate trap

As was discussed, different trap geometries are expected to result in different collapse dynamics. So figures 2 and 3 have to be compared with the time evolution of an almost spherical and a pancake-shaped trap. While the collapse in an almost spherical trap has been published in [32], we present the pancake-shaped trap in figure 4.

The pancake-shaped trap is formed by superimposing two additional lattice beams onto a condensate, which was produced in the crossed dipole trap, see figure 1. Depending on the non-stabilized relative phase of the two lattice beams, it is in principle possible that the condensate

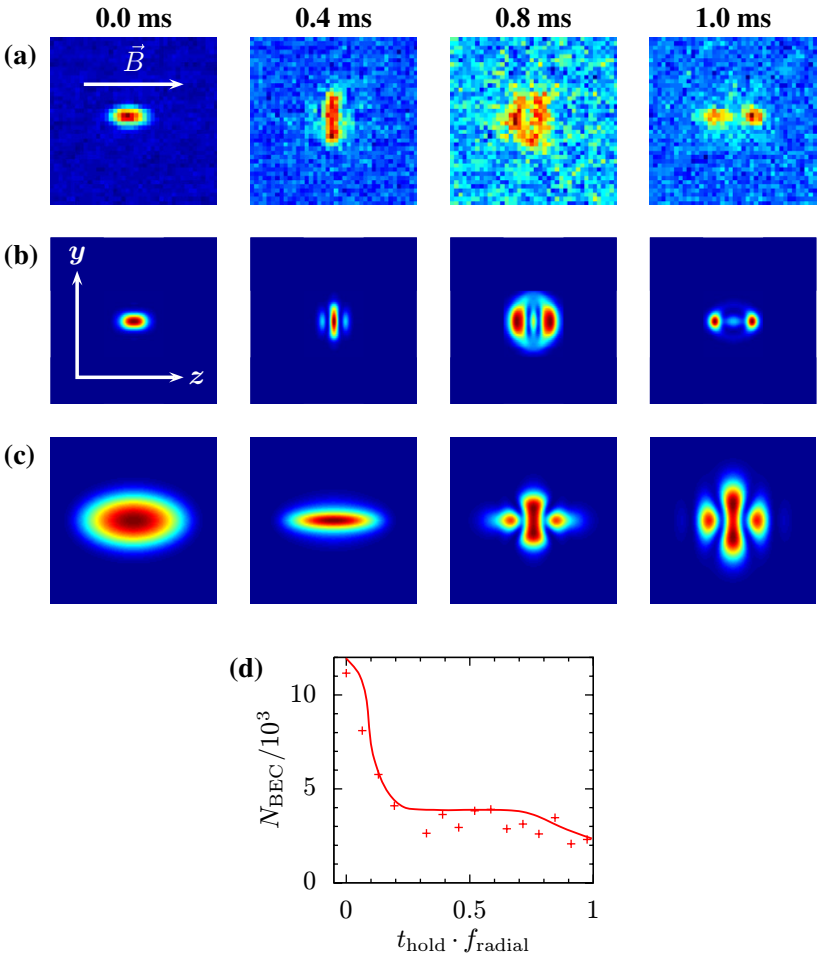

Figure 3. (a, b) Collapse dynamics for different holding times t_{hold} in a weakly cigar-shaped trap with trap frequencies $(f_x, f_y, f_z) \approx (650, 520, 400)$ Hz, trap ratio $\lambda \approx 0.7$ and radial trap period $\tau \sim 1.7$ ms. Each picture is a single absorption image after 8 ms of time-of-flight and has its own optical density scale. The field of view is $250 \times 250\,\mu\mathrm{m}^2$. (c) Simulated in-trap absorption images. The field of view is $6.9 \times 6.9\,\mu\mathrm{m}^2$. (d) N_{BEC} versus t_{hold}. The solid line is the simulation result.

splits into two. Practically, we have never observed interference fringes, even at expansion times long enough, so that the fringe spacing $ht_{\mathrm{tof}}/(md_{\mathrm{lat}})$ was larger than our 6 μm resolution limit. Switching off the trapping potential immediately after finishing the magnetic field ramp results in a highly elongated condensate, in agreement with the simulations (figure 4).

The cylindrical symmetry of the pancake-shaped trap allows us to recover the 3D density distribution $n(\rho, z)$ from the 2D absorption image $n_{\mathrm{abs}}(y, z)$. Figures 4(d) and (e) show isodensity surfaces for two different densities obtained from the inverse Abel transformation [33]

$$n(\rho, z) = \frac{1}{2\pi} \int_0^\infty \mathrm{d}k k J_0(k \cdot \rho) \int_{-\infty}^{\infty} \mathrm{d}y\, n_{\mathrm{abs}}(y, z) \exp(-\mathrm{i}ky) \tag{3}$$

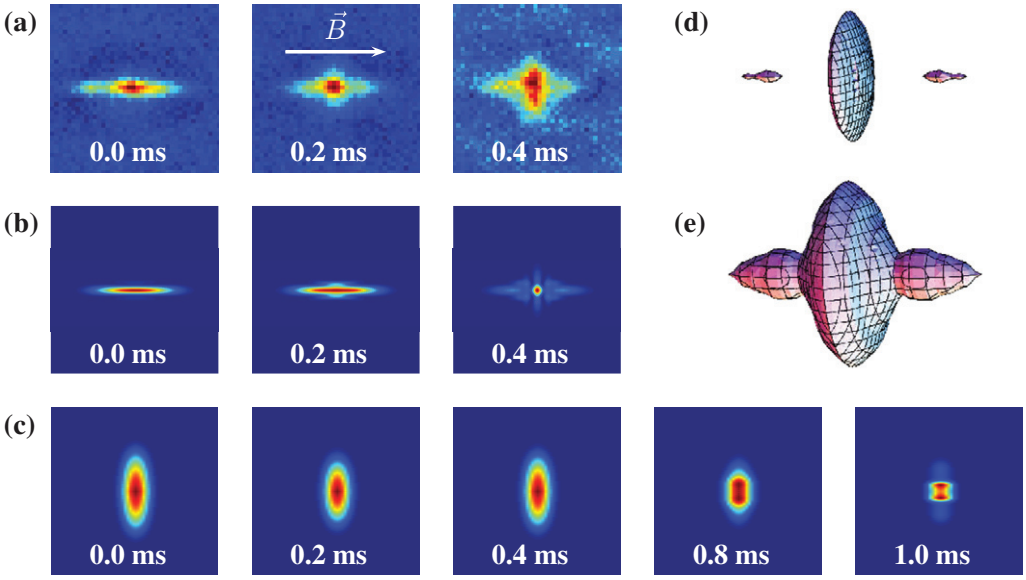

Figure 4. (a, b) The collapse dynamics for different holding times t_{hold} in a pancake-shaped trap, which corresponds to trap frequencies $(f_x, f_y, f_z) \sim (400, 400, 3400)$ Hz, trap ratio $\lambda \approx 8.5$ and radial period $\tau \simeq 2.5$ ms. The upper row presents the average of five absorption images after 8 ms of free expansion. The final ramp starts at $a_{\mathrm{i}} = (30 \pm 2)a_{\mathrm{Bohr}}$ and stops at $a_{\mathrm{f}} = (-13 \pm 2)a_{\mathrm{Bohr}}$. The simulations give $a_{\mathrm{crit}} = (-1.5 \pm 0.5)a_{\mathrm{Bohr}}$. (c) Simulated in-trap absorption images. The field of view is $(y, z) = (8.9, 4.5)$ μm. Isodensity surfaces for 'high' (d) and 'low' (e) densities of the $t_{\mathrm{hold}} = 0.4$ ms image obtained from the Abel transformation.

for $t_{\mathrm{hold}} = 0.4$ ms, where J_0 is the Bessel function of the first kind. As in the almost spherical trap [32], the collapsed cloud exhibits a d-wave symmetry. While the isodensity surface for 'high' densities contains a central disc and two separated 'blobs' along the symmetry axis, the three parts merge for 'low' densities. Because the Abel transformation is very sensitive to noise, we cannot extract in a reliable way from our images the kinetic energy released during the collapse.

4. Testing the coherence of the collapsed cloud

By analyzing the collapse of condensates confined in different trap geometries, we showed that the survival density pattern exhibits two parts: one part which is well described by a thermal cloud, and a second part, which, due to its high optical density, we interpreted as a remnant condensate [32]. In order to confirm this interpretation, we checked the coherence of interfering condensates in the case of pancake-shaped traps.

For that purpose, we produce several condensates by superimposing the two beams for the optical lattice *before* finishing the evaporation to reach quantum degeneracy. Here the extension of the cloud is still large enough, so that the atoms occupy three to five adjacent lattice sites. The exact number of occupied sites changes from shot to shot, depending on the relative phase of the two lattice beams, which are not actively stabilized. After condensing, the BECs on different

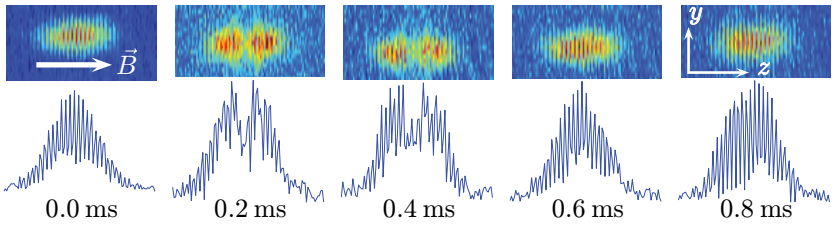

Figure 5. Interference pattern of three to five independent condensates for different holding times t_{hold} in the pancake-shaped trap, $(f_x, f_y, f_z) \sim (400, 400, 3400)$ Hz. The lower graphs show the y-integrated column densities $\sum_y \int \mathrm{d}\,x\,|\psi|^2$ (time-of-flight 18 ms, field of view $110 \times 690\ \mu\mathrm{m}^2$).

lattice sites have random phases with respect to each another. The single-particle tunneling rate is vanishingly small ($< 10^{-30}\ \mathrm{s}^{-1}$), so that no phase coherence between adjacent sites is built up on the timescale of the experiment.

It is known [34] that the interference fringes are not washed out if a few independent condensates interfere instead of only two. Taking the same trap geometry as in figure 4, but extending the time-of-flight to 18 ms, we obtain the interference patterns shown in figure 5. As expected, the absolute position of the interference fringes changes from shot to shot, but can be clearly seen on each image.

While for holding times shorter than 0.2 ms or longer than 0.5 ms, interference fringes with a high contrast are visible, we observe no interference fringes at the center of the two clouds for $0.2\,\mathrm{ms} \leqslant t_{\mathrm{hold}} \leqslant 0.5\,\mathrm{ms}$. A possible interpretation is as follows: for $t_{\mathrm{hold}} = 0\,\mathrm{ms}$, *no* collapse occurs and the observed fringes are similar to those of two-point sources. For $t_{\mathrm{hold}} = 0.2$ and 0.4 ms the condensates do collapse, but this happens during the time-of-flight and *after* the clouds overlapped; for example, for $t_{\mathrm{hold}} = 0.4\,\mathrm{ms}$ the condensates start to overlap for $t_{\mathrm{tof}} = 0.4\,\mathrm{ms}$, but the collapse happens at $t_{\mathrm{tof}} = 0.8\,\mathrm{ms}$. Probably this induces a complicated phase distribution in each of the condensates and integration over the line of sight washes out the interference fringes. On the other hand, if the collapse happens in-trap (e.g. for $t_{\mathrm{hold}} = 0.8\,\mathrm{ms}$), the fringes are formed by the remnant condensates. Again we recover the fringes as if the atoms belonged to two coherent point sources.

5. Conclusions

We have investigated theoretically and experimentally the collapse dynamics of dipolar condensates in prolate and oblate harmonic trapping potentials. As expected, the collapse dynamics depends on the trap geometry, although the qualitative behavior is similar for different traps. The simulations containing no adjustable parameter reproduce the experimental results well. By simultaneously inducing a collapse in several condensates and allowing them to interfere, we showed that the collapsed cloud contains a coherent remnant condensate.

A clear direction of further studies is to use the interferometric technique of section 4 to obtain experimental evidence for the vortex rings predicted in [32]. The contrast of the interference fringes is not high enough to support their evidence yet. Another interesting extension is the study of 2D solitons [35, 36], which are expected to appear just above the instability threshold.

Acknowledgments

We acknowledge support from the German Research Foundation (SFB/TRR 21), the Landesstiftung Baden-Württemberg and the EU (Marie-Curie grant number MEIF-CT-2006-038959 to TL). HS, YK and MU acknowledge support from the Ministry of Education, Culture, Sports, Science and Technology of Japan (Grants-in-Aid for Scientific Research numbers 17071005 and 20540388 and the Global COE Program 'the Physical Sciences Frontier') and by the Matsuo Foundation.

References

[1] Woosley S E, Heger A and Weaver T A 2002 *Rev. Mod. Phys.* **74** 1015–71
[2] Fattori M, Roati G, Deissler B, D'Errico C, Zaccanti M, Jona-Lasinio M, Santos L, Inguscio M and Modugno G 2008 *Phys. Rev. Lett.* **101** 190405
[3] Levy S, Lahoud E, Shomroni I and Steinhauer J 2007 *Nature* **449** 579–83
[4] Greiner M, Mandel O, Esslinger T, Hänsch T W and Bloch I 2002 *Nature* **415** 39–44
[5] Billy J, Josse V, Zuo Z, Bernard A, Hambrecht B, Lugan P, Clément D S, Sanchez-Palencia L, Bouyer P and Aspect A 2008 *Nature* **453** 891–4
[6] Paredes B, Widera A, Murg V, Mandel O, Fölling S, Cirac I, Shlyapnikov G V, Hänsch T W and Bloch I 2004 *Nature* **29** 277–81
[7] Kinoshita T, Wenger T and Weiss D S 2004 *Science* **305** 1125–8
[8] Hadzibabic Z, Krüger P, Cheneau M, Battelier B and Dalibard J 2006 *Nature* **441** 1118–21
[9] Bloch I, Dalibard J and Zwerger W 2008 *Rev. Mod. Phys.* **80** 885–964
[10] Gerton J M, Strekalov D, Prodan I and Hulet R G 2000 *Nature* **408** 692–5
[11] Donley E A, Claussen N R, Cornish S L, Roberts J L, Cornell E A and Wieman C E 2001 *Nature* **412** 295–9
[12] Dalfovo F, Giorgini S, Pitaevskii L P and Stringari S 1999 *Rev. Mod. Phys.* **71** 463–512
[13] Baranov M, Dobrek L, Góral K, Santos L and Lewenstein M 2002 *Phys. Scr.* **T102** 74–81
[14] Góral K, Santos L and Lewenstein M 2002 *Phys. Rev. Lett.* **88** 170406
[15] Baranov M 2008 *Phys. Rep.* **464** 71–111
[16] Santos L, Shlyapnikov G V and Lewenstein M 2003 *Phys. Rev. Lett.* **90** 250403
[17] O'Dell D H J, Giovanazzi S and Eberlein C 2004 *Phys. Rev. Lett.* **92** 250401
[18] Ronen S, Bortolotti D C E and Bohn J L 2007 *Phys. Rev. Lett.* **98** 030406
[19] Dutta O and Meystre P 2007 *Phys. Rev.* A **75** 053604
[20] Yi S and Pu H 2006 *Phys. Rev.* A **73** 061602
[21] Cooper N R, Rezayi E H and Simon S H 2005 *Phys. Rev. Lett.* **95** 200402
[22] Zhang J and Zhai H 2005 *Phys. Rev. Lett.* **95** 200403
[23] Kawaguchi Y, Saito H and Ueda M 2006 *Phys. Rev. Lett.* **96** 080405
[24] Santos L and Pfau T 2006 *Phys. Rev. Lett.* **96** 190404
[25] Yi S and Pu H 2006 *Phys. Rev. Lett.* **97** 020401
[26] Koch T, Lahaye T, Metz J, Fröhlich B, Griesmaier A and Pfau T 2008 *Nat. Phys.* **4** 218–22
[27] Stuhler J, Griesmaier A, Koch T, Fattori M, Pfau T, Giovanazzi S, Pedri P and Santos L 2005 *Phys. Rev. Lett.* **95** 150406
[28] Lahaye T, Koch T, Fröhlich B, Fattori M, Metz J, Griesmaier A, Giovanazzi S and Pfau T 2007 *Nature* **448** 672–5
[29] Saito H and Ueda M 2002 *Phys. Rev.* A **65** 033624
[30] Werner J, Griesmaier A, Hensler S, Stuhler J, Pfau T, Simoni A and Tiesinga E 2005 *Phys. Rev. Lett.* **94** 183201
[31] Köhler T, Góral K and Julienne P S 2006 *Rev. Mod. Phys.* **78** 1311–61

[32] Lahaye T, Metz J, Fröhlich B, Koch T, Meister M, Griesmaier A, Pfau T, Saito H, Kawaguchi Y and Ueda M 2008 *Phys. Rev. Lett.* **101** 080401
[33] Bracewell R N 2000 *The Fourier Transfrom and its Applications* (New York: McGraw-Hill)
[34] Hadzibabic Z, Stock S, Battelier B, Bretin V and Dalibard J 2004 *Phys. Rev. Lett.* **93** 180403
[35] Pedri P and Santos L 2005 *Phys. Rev. Lett.* **95** 200404
[36] Tikhonenkov I, Malomed B A and Vardi A 2008 *Phys. Rev. Lett.* **100** 090406